Aerosol and Air Quality Research, 17: 2645–2658, 2017

ISSN: 1680-8584 print / 2071-1409 online
doi: 10.4209/aaqr.2016.12.0554

Numerical Simulation and Experimental Validation for the Filtration Performance of Fibrous Air Filter Media with LB Method

Bin Zhou*, Yang Xu, Jia-Qi Fan, Li-Ping Chen, Fei Li, Ke Xue

Department of HVAC, College of Urban Construction, Nanjing Tech University, Nanjing 210009, China

ABSTRACT

The performance of fibrous air filter media is one of the key factors to influence the indoor air quality. In order to develop low-resistance and high-efficiency media, it is necessary to obtain a realistic media model. Based on the truncated log-normal model, the D2G9 scheme of Lattice Boltzmann (LB) method was applied to predict both the resistance and the filtration efficiency of the flow through microscale porous media. The influences of the boundary conditions were investigated. The slip and no-slip boundary conditions on fiber surfaces, as well as the non-equilibrium extrapolation scheme and the periodic scheme, were included in this study. By validating the simulated results with both the experimental and empirical values, it was found that the simulated resistance with the slip boundary on fiber surface and the periodic scheme on upper/lower walls was closer to the real value. The model established in this paper and the LB method presented here provide support for further research on optimization of the fibrous air filter media.

Keywords: Fibrous media; LB method; Slip boundary condition; Resistance; Efficiency.

NOMENCLATURE

Abbreviations

BSR	bounce-back/specular-reflection
LB	Lattice Boltzmann
LBE	Lattice Boltzmann equation

Latin Letters

A	cross-sectional area, (m^2)
A_1	first-order slip coefficient
A_2	second-order slip coefficient
C	propagation speed (= δ_x/δ_t)
C_c	relaxation time of particles, (s)
c_s	lattice sound speed (= $1/\sqrt{3}\cdot\delta_x/\delta_t$ in D2Q9 model)
d_p	particle diameter, (m)
$f_\alpha(\boldsymbol{r}, t)$	distribution function at position $\boldsymbol{r}$ and time t along the direction α
$f_\alpha^{eq}(\boldsymbol{r},t)$	equilibrium distribution function at position $\boldsymbol{r}$ and time t along the direction α
F_B	Brownian force per unit particle mass, (m s^{-2})
F_D	drag force by fluid per unit particle mass, (m s^{-2})
k_B	Boltzmann constant, (J K^{-1})
Kn	Knudsen number
L	filter media thickness, (m)
N	the wall normal coordinate pointing into the fluid
N	mesh number of a characteristic length
NY	number of lattices along y direction
p_{in}	static pressure at inlet of media, (Pa)
p_{out}	static pressure at outlet of media, (Pa)
Q	flow rate through the filter media, ($m^3\cdot s^{-1}$)
R	gas constant, (J mol^{-1} K^{-1})
R_f	average diameter of fibers, (m)
r_b	a parameter to measure slippage degree ($0 \le r_b \le 1$)
t	time, (s)
T	absolute temperature, K
u_p	particle velocity, (m s^{-1})
u_s	slip velocity, (m s^{-1})
U	inlet velocity, (m s^{-1})

Greek Letters

δ_t	discrete time step, (s)
τ	relaxation time, (s)
τ_p	relaxation time of particle (= $\rho_p\cdot d_p\cdot d_p\cdot C_s/18\mu$, s)
μ	dynamic viscosity of the gas, (kg m^{-1} s^{-1})
υ	kinematic fluid viscosity, (m^2 s^{-1})
δ_x	discrete lattice step, (m)
ρ_0	average density of the fluid, (kg m^{-3})
ρ_p	particle density, (kg m^{-3})
α	solid volume fraction
ξ	Gaussian random variable
Δt	time step for the movement of particles, (s)
Δp	pressure drop through fibrous filter media, (Pa)
$\Delta p_{no\text{-}slip}$	pressure drop with no-slip boundary, (Pa)
Δp_{slip}	pressure drop with slip boundary condition, (Pa)

* Corresponding author.
Tel.: 86-13404144095; Fax: 86-25-83239533
E-mail address: bin.zhou@njtech.edu.cn; zhoubinwx@hotmail.com

INTRODUCTION

Air filtration is a major concern in many sectors of industry such as hospital, clean operating rooms and automotive cabin (Kim *et al*., 2016). Fibrous air filter is currently one of the most economical and effective ways, which has been widely applied. The performance of filter media is crucial to the performance of filter, since it is related to the energy consumption and efficiency of HVAC system. It is therefore essential to be able to predict the performance of the fibrous air filter media with appropriate models.

There are many analytical, numerical and empirical models that have been developed for fibrous media made up of circular fibers (Tronville and Rivers, 2005; Hosseini and Tafreshi, 2011; Joubert *et al*., 2011; Fotovati *et al*., 2012; Qian *et al*., 2013; Zhou *et al*., 2013; Xu *et al*., 2014). Some researchers have found that fluids flowing past fiber surfaces experience a slip which could reduce the flow resistance in a microscale channel. The slip phenomenon in porous media has been vastly studied in recent literatures (Zhao and Povitsky, 2009; Hosseini and Tafreshi, 2010; Chai *et al*., 2011; Hosseini and Tafreshi, 2011; Kirsh and Shabatin, 2015).

Recently, the Lattice Boltzmann equation (LBE), a discrete version of the continuous Boltzmann equation which can capture non-equilibrium gas flows, has been considered as a promising numerical approach for microscale gas flows (Tang *et al*., 2005; Kim *et al*., 2008; Przektop and Gradon, 2008; Agarwal *et al*., 2009; Chen *et al*., 2009; Wang *et al*., 2009; Neumann and Rohrmann, 2012; Cho *et al*., 2013; Bang and Yoon, 2014). The gas flow in the microscale channels has a big difference from the conventional situation. *Kn* number is a parameter used to determine the rarefaction of gas flow and whether there exists slip phenomenon on the surface. Based on *Kn* number, the flow could be classified into the regimes as follows, i.e., the continuum regime ($Kn \leq 0.001$), the slip flow regime ($0.001 < Kn \leq 0.1$), the transitional regime ($0.1 < Kn \leq 10$), and the free molecular regime ($Kn > 10$) (Zheng *et al*., 2012). When the flow enters the slip flow regime, the slip phenomenon occurs. In other words, the slip velocity should physically increase with the increase of *Kn*. The slip effects imposed at a solid-fluid interface were well captured by the current LB method. Two mesoscopic kinetic boundary conditions are widely used to realize the slip boundary conditions, i.e., the combination of bounce-back and specular reflection (BSR) scheme (Przekop and Gradoń, 2008; Guo *et al*., 2002; Succi, 2002; Tang *et al*., 2004; Sbragaglia and Succi, 2005) and the discrete Maxwellian (DM) scheme (Ansumali and Karlin, 2002; Niu *et al*., 2004; Tang *et al*., 2005; Zheng *et al*., 2012). Guo *et al*. (2002) also pointed out that BSR and DM schemes are useful for different applications. Zheng *et al*. (2012) analyzed three kinds of microboundary schemes, i.e., BSR, combination of Maxwell and bounce-back (MB) and combination of Maxwell and specular reflection (MR) schemes, to show how to choose the combination coefficients in these mathematical expressions.

Yamamoto *et al*. (2009) and Yamamoto and Yamauchi, (2013) investigated the flow field and particle capture process in diesel particulate filter by using LBM. They found that after particle deposited on filter, the flow field was different from the initial condition. Przekop and Gradoń (2011) studied the non-steady-state process of particle capture in the fibrous media, where the dentrite shape formed on fiber surface by capture particles was investigated. By applying LBM, Rebaï *et al*. (2011) compared the random fibrous media models with single fiber diameter and dual fiber diameters. They found that under fixed flow rate and pressure drop, the filtration performance of fibrous media with larger porosity and larger weight was better than that with less fibers. Wang *et al*. (2012) investigated the initial pressure drop and efficiency of multiple circular fibers, as well as the particle loading process. Later they studied the parallel and staggered fibrous media models (Wang *et al*., 2013). They found that the performance of staggered model is better than that of parallel model. Huang *et al*. (2016) investigated the performance of the noncircular fibers, including pressure drop and collection efficiency in the diffusion dominant regime with LBM. They found that the pressure drop is related to the aspect ratio and the orientation angle.

However, the investigations of slip phenomenon on fiber surface and its influence on filtration performance of filter media are still rare. In a fibrous filter, aerodynamic slip takes place when the fiber diameter is comparable to the mean free path of the gas molecules. In this case, collisions between the gas molecules and the fibers become so infrequent that the gas can no longer be treated as a continuum phase with respect to the fibers (Hosseini and Tafreshi, 2011). Moreover, the Cunningham slip factor should be considered in the model for particles with diameter near 1 μm.

Therefore, in this study the truncated log-normal distributed model (Zhou *et al*., 2009) will be investigated by using LB method when slip boundary condition is considered. Both the initial pressure drop and the filtration efficiency will be investigated, which is aimed to provide a feasible theoretical and numerical model for further study of fibrous air filter media with low-resistance and high-efficiency.

MATHEMATICAL MODEL

Computational Model

The computational domain and the log-normal distributed random fiber model (Zhou *et al*., 2009) were adopted, which represents the image of a cutting plane perpendicular to the filter media. Modeling selects only a small fraction of the total width, but includes the entire thickness, taking explicit account of the microstructure and the variability of fibers in both diameter and location. Fiber diameters were sampled by measuring the width of those fibers intersected by straight lines drawn at random across the image. The media was modeled with realistic descriptions of real structures of filters, where circles are randomly spaced by C++ programs. It provides an accurate model basis for simulating the microscopic flow conditions in media samples.

The schematic diagram of media F6 model is illustrated in Fig. 1. The media thickness L = BC, and the media width W = CF. The width was set to be 75 μm. The distance from the inlet to the media AB = 120 μm which was set to ensure that the velocity field at the windward side of the media

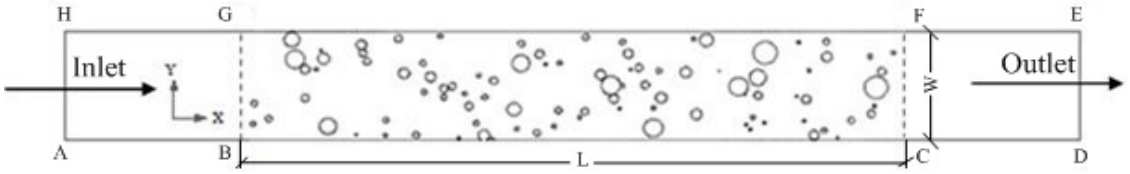

Fig. 1. The two-dimensional cross section of media F6.

(Line BG in Fig. 1) was not affected by the influence of inlet flow. Likewise, the distance from the outlet to the media CD = 120 μm which was set to prevent the inverse flow for the full development of the air flow in the media. The sensitivity analysis of media thickness and width has been performed and the optimal values are adopted (Zhou *et al*., 2009). In Table 1, the geometric information is presented for the media model.

Lattice Boltzmann Method

LB method is a discrete process in macro, but a continuous process in micro. Therefore, LB method is called mesoscopic simulation method. It provides the possibility and reality to link macro and micro, and it also sets an effective way for simulating the porous media flow as well. In this paper, the D2G9 scheme of LB method on a two-dimensional square lattice was adopted, which can simulate incompressible fluid flow accurately and efficiently (He *et al*., 2009). The evolution of fluid particles can be decomposed into migration and collision processes. The code was compiled by C++ programs.

The evolution of the distribution function $f_\alpha(\boldsymbol{r}, t)$ also obeys the Lattice Boltzmann equation:

$$f_\alpha(\mathbf{x}+\mathbf{e}_\alpha\delta_t, t+\delta_t) - f_\alpha(\mathbf{x},t) = -\frac{1}{\tau}[f_\alpha(\mathbf{x},t) - f_\alpha^{eq}(\mathbf{x},t)] \quad (1)$$

where $\delta_t = 1$ is the discrete time step and f_α^{eq} is the equilibrium distribution function.

In D2Q9 model, nine velocities e_α were defined as e_0 = 0, and e_α = {cos[(i– 1)π/2], sin[(i – 1)π/2]} for α = 1–4 and $e_\alpha = \sqrt{2}$ {cos[(i – 5)π/2], sin[(i – 5)π/2]} for α = 5–8.

In kinetic theory, the kinematic fluid viscosity υ can be defined as (Tian *et al*., 2009):

$$\upsilon = \frac{1}{2}\sqrt{\frac{8RT}{\pi}} KnN\delta_x \quad (2)$$

The kinematic fluid viscosity υ was given as (He *et al*., 2009):

$$\upsilon = c_s^2(\tau - 0.5)\delta_t \quad (3)$$

where the lattice speed of sound $c_s = (1/\sqrt{3})c = (1/\sqrt{3})\delta x/\delta t$. For the two-dimensional and nine-speed LB models, $c_s = \sqrt{RT}$.

In Eq. (2), the dimensionless relaxation time τ can be derived from Eq. (4), which was widely used in simulating microscale air flows with LB method (Zheng *et al*., 2012):

$$\tau = \frac{1}{2} + \sqrt{\frac{6}{\pi}}\frac{Kn}{\Delta} \quad (4)$$

where $\Delta = 1/N = \delta_x/L$, N is the mesh number of a characteristic length; δ_x is the discrete lattice step (He *et al*., 2009). In Eq. (4), the average Kn number in Table 2 was taken, so that LB models can be applied to simulate microscale air flows (Tian *et al*., 2009).

The equilibrium distribution function $f_\alpha^{eq}(\mathbf{x},t)$ was redefined as the form of Guo's incompressible model (He *et al*., 2009):

$$f_\alpha^{eq} = \begin{cases} \rho_0 - 4d_0\dfrac{p}{c^2} + \rho_0 s_0(\mathbf{u}) & \alpha = 0 \\ d_1\dfrac{p}{c^2} + \rho_0 s_\alpha(\mathbf{u}) & \alpha = 1,2,3,4 \\ d_2\dfrac{p}{c^2} + \rho_0 s_\alpha(\mathbf{u}) & \alpha = 5,6,7,8 \end{cases} \quad (5)$$

where constant ρ_0 was the average density of the fluid; s_α was defined as follows:

$$s_\alpha(\mathbf{u}) = w_\alpha\left[\frac{\mathbf{e}_\alpha\cdot\mathbf{u}}{c_s^2} + \frac{(\mathbf{e}_\alpha\cdot\mathbf{u})^2}{2c_s^4} - \frac{\mathbf{u}^2}{2c_s^2}\right] \quad (6)$$

Table 1. The geometric information of the media model.

Parameters / Media sample	Rated velocity (m s^{-1})	Thickness(L) × Width (W) (μm)	Number of cylinders	Solid fraction (α)	d_f (μm)
F6	0.0617	430 × 75	101	7.57%	1.17–15.22

Table 2. The *Kn* ranges of filter media F6.

Kn Range	0.001–0.01	0.01–0.1	0.1–10	Average *Kn*	*Kn* for lower diameter limit	*Kn* for upper diameter limit
F6	22.77%	77.23%	0	0.0193	0.057	0.004

d_0, d_1 and d_2 were model parameters, which were given by:

$$\begin{cases} d_1 + d_2 = d_0 \\ d_1 + 2d_2 = \dfrac{1}{2} \end{cases} \tag{7}$$

In the numerical simulation, d_0, d_1 and d_2 can be chosen as 5/12, 1/3 and 1/12, respectively (Li *et al*., 2015).

The weight coefficient w_α was defined as:

$$w_\alpha = \begin{cases} 4/9 & (i = 0) \\ 1/9 & (i = 1,2,3,4) \\ 1/36 & (i = 5,6,7,8) \end{cases} \tag{8}$$

In the process of evolution, it is required to maintain the conservation of mass and momentum, namely:

$$\rho_0 = \sum_\alpha f_\alpha = \sum_\alpha f_\alpha^{eq}, \ \rho_0 \mathbf{u} = \sum_\alpha \mathbf{e}_\alpha f_\alpha = \sum_\alpha \mathbf{e}_\alpha f_\alpha^{eq} \tag{9}$$

Macroscopic pressure of the fluid could be obtained from Eq. (10).

$$p = \frac{c^2}{4d_0}[\sum_{\alpha \neq 0} f_\alpha + s_0(\mathbf{u})] \tag{10}$$

With the Chapman-Enskog expansion, the macroscopic equation of D2G9 model can be used to derive the full N-S equations.

For describing the movement of airborne particles, the CA probability model was applied. Both the drag force and Brownian diffusion on particles were considered. Eqs. (11) and (12) were used to obtain the variation of particle velocity and position, respectively.

$$\frac{d\mathbf{u}_p}{dt} = \mathbf{F}_D + \mathbf{F}_B = \frac{\mathbf{u} - \mathbf{u}_p}{\tau_p} + \xi\sqrt{\frac{216\mu k_B T}{\pi \rho_P^2 d_p^5 \Delta t}} \tag{11}$$

$$\frac{d\mathbf{x}_p}{dt} = \mathbf{u}_p \tag{12}$$

where u_p is the particle velocity; τ_p is the relaxation time of particle, $\tau_p = \dfrac{\rho_p d_p^2 C_c}{18\mu}$; C_c is the relaxation time with the expression $C_c = 1 + \lambda/d \times [2.34 + 1.05 \times \exp(-0.39 \times d/\lambda)]$; ρ_p is the particle density; d_p is the particle diameter; F_B is the random Brownian force; F_D is the drag force by the fluid; k_B is the Boltzmann constant; μ is the dynamic viscosity of the gas; T is the thermodynamic temperature; ξ is the Gaussian random variable with average value 0 and variance 1; Δt is the time step for the movement of particles.

By integration of Eqs. (11) and (12), Eqs. (13) and (14) were obtained.

$$\mathbf{u}_p^{n+1} = \mathbf{u}_p^n \exp(-\frac{\Delta t}{\tau_p}) + (\mathbf{u}_f + \mathbf{F}_B \tau_p)\left[1 - \exp(-\frac{\Delta t}{\tau_p})\right] \tag{13}$$

$$\begin{aligned} \mathbf{x}_p^{n+1} = \mathbf{x}_p^n + \left(\mathbf{u}_p^n - \mathbf{u}_f\right)\left[1 - \exp(-\frac{\Delta t}{\tau_p})\right]\tau_p + \mathbf{u}_f \Delta t \\ + \left\{\Delta t + \left[1 - \exp(-\frac{\Delta t}{\tau_p})\tau_p\right]\right\}\mathbf{F}_B \tau_p \end{aligned} \tag{14}$$

where the superscript n denotes the current time; $n + 1$ denotes the next step.

Boundary Condition

Slip Boundary Condition

In order to estimate the possibility of slip phenomenon taking place on the given fibers' surface, the range of the fiber diameter was needed to be known. According to the measured fiber diameter data, the values corresponding to each *Kn* range are illustrated in Table 2.

It can be seen that the *Kn* of all fibers range from 0.001 to 0.1, where N-S equation with slip boundary conditions may be applied to flows in slip flow regime or marginally transitional regime. For filter media F6, all fibers can be considered in the slip flow regime. Table 2 shows that no fiber is in free molecular flow regime.

In this paper, the slip velocities on all the fiber surfaces were implemented by the boundary condition combining the bounce-back with the specular reflection (BSR scheme), which was proposed by Succi (2002). Here, taking the wall boundaries for example, the BSR scheme can be described as follows (Tang *et al*., 2004).

At bottom wall of fibers (arc I-L-J in Fig. 2):

$$\begin{aligned} f_2(x,0) &= f_4(x,0) \\ f_5(x,0) &= r_b f_7(x,0) + (1 - r_b) f_8(x,0) \\ f_6(x,0) &= r_b f_8(x,0) + (1 - r_b) f_7(x,0) \end{aligned} \tag{15}$$

At top wall of fibers (arc I-K-J in Fig. 2):

$$\begin{aligned} f_4(x,NY) &= f_2(x,NY) \\ f_7(x,NY) &= r_b f_5(x,NY) + (1 - r_b) f_6(x,NY) \\ f_8(x,NY) &= r_b f_6(x,NY) + (1 - r_b) f_5(x,NY) \end{aligned} \tag{16}$$

where NY is the number of lattices in y direction, and the proportion coefficient r_b is a parameter to measure slippage

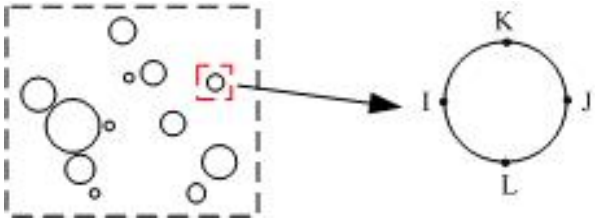

Fig. 2. The diagram of a fiber inside fibrous media.

degree ($0 \le r_b \le 1$). In other words, r_b and $1 - r_b$ represents the probability for a fluid particle to be bounced back and slipped forward, respectively. When $r_b = 1$, it corresponds to pure bounce-back scheme, which means that a fluid particle changes its moving direction to the opposite one when it contacts the solid surface (Przekop and Gradoń, 2008). Whereas $r_b = 0$ corresponds to pure specular reflection scheme used for free slip boundary conditions. Tang adopted $r_b = 0.7$, which was used to best capture the slip-velocity on the solid-gas wall, i.e., more fluid particles will be reflected in the backward direction than the forward direction. Tang also pointed out that the value of r_b was probably *Kn* number dependent and $r_b = 0.7$ worked well for the present *Kn* number range (0.055–0.16) as the predicted flow results were shown to be closer to the available data (Tang *et al*., 2004). For the *Kn* ranges of filter media F6, the value of r_b was needed to be recalculated.

In the slip flow regime ($0.001 < Kn \le 0.1$), the commonly used second-order slip boundary condition takes the form (He *et al*., 2009):

$$u_s = A_1 \lambda \left.\frac{\partial u}{\partial n}\right|_w - A_2 \lambda^2 \left.\frac{\partial^2 u}{\partial n^2}\right|_w \tag{17}$$

where u_s is the slip velocity; A_1 and A_2 are the first-order and second-order slip coefficients; n is the wall normal coordinate pointing into the fluid; the subscript w represents the quantity at the wall. Hadjiconstantinou rescaled the values of A_1 and A_2 considering Knudsen layer effects and obtained $A_1 = 1.11$ and $A_2 = 0.61$, respectively (Hadjiconstantinou, 2003).

Parameter r_b of BSR scheme is chosen as (He *et al*., 2009):

$$r_b = \left\{1 + \sqrt{\frac{\pi}{6}}\left[\frac{\Delta^2}{4Kn} + A_1 + (2A_2 - \frac{8}{\pi})Kn\right]\right\}^{-1} \tag{18}$$

Bounce-Back Boundary Condition

In order to reflect the slippage effects, the no-slip boundary conditions were considered by an improved bounce-back scheme with second-order accuracy. For standard bounce-back scheme, the distribution function of boundary nodes can be obtained by the relative fluid nodes after bounce-back:

$$f_2 = f_4, f_5 = f_7, f_6 = f_8 \tag{19}$$

To satisfy the no-slip condition, the distribution functions f_α can take the following expressions as Eq. (20). Take the bottom wall for example:

$$\begin{aligned} f_2 &= f_4 \\ f_5 &= f_5 - \frac{1}{2}\rho(u+v) \\ f_6 &= f_6 + \frac{1}{2}\rho(u-v) \end{aligned} \tag{20}$$

The velocity boundary condition was applied to the inlet, whereas the fully developed format was used for the outlet boundary.

Non-Equilibrium Extrapolation Boundary

Guo *et al*. (2002) proposed the non-equilibrium extrapolation boundary in 2002, which has a second order accuracy in time and space. In Fig. 3, C/O/A is the solid boundary, and the node E/B/D is the fluid node located in flow field.

The distribution function collision at point O can be approximated as follows.

$$f_\alpha(O,t) = f_\alpha^{eq}(O,t) + [f_\alpha(B,t) - f_\alpha^{eq}(B,t)] \tag{21}$$

When the collision process is considered, the distribution function collision at point O after collision can be expressed as:

$$f_\alpha^+(O,t) = f_\alpha^{eq}(O,t) + (1 - \frac{1}{\tau})[f_\alpha(B,t) - f_\alpha^{eq}(B,t)] \tag{22}$$

$$\begin{aligned} f_2 &= f_4 \\ f_5 &= f_5 - \frac{1}{2}\rho(u+v) \\ f_6 &= f_6 + \frac{1}{2}\rho(u-v) \end{aligned} \tag{23}$$

In cases A and B in Table 4, both the upper and the lower boundaries adopted non-equilibrium extrapolation format.

Periodic Boundary

The periodic boundary means that when the fluid particles leave from one side of the flow field, they will enter into the flow field from the other side at the next step. Therefore, this boundary treatment can strictly ensure the conservation of mass and momentum of the entire system.

The treatment of the periodic boundary can be given as follows.

$$f_{1,5,8}(0, j) = f_{1,5,8}(N_x, j) \tag{24}$$

$$f_{3,6,7}(N_x + 1, j) = f_{1,5,8}(1, j) \tag{25}$$

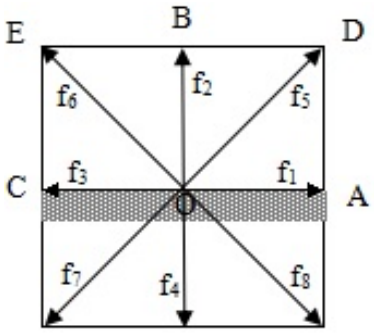

Fig. 3. The scheme of non-equilibrium extrapolation boundary.

where the expression $f_{1,5,8}(0, j) = f_{1,5,8}(N_x, j)$ represents that the equilibrium distribution functions f_1, f_5 and f_8 of the virtual fluid node $(0, j)$ were equal to that of the fluid node (N_x, j). Cases C and D in Table 4 both corresponded to the situation when the upper and lower boundaries adopted periodic boundary format.

Theoretical Expressions for Resistance

For fibrous filter media, the resistance Δp is related to the following variables: the flow rate Q, the cross-sectional area A, the media thickness L, the dynamic viscosity μ, the density ρ, the mean free path of air molecules λ, the solid volume fraction α, and the average diameter of fibers R_f.

According to Davies' theory, when the resistance Δp is quite small, the following relationship can be obtained (Davies, 1973):

$$\frac{\Delta pA(R_f)^2}{\mu QL} = f(\alpha) \tag{26}$$

where $f(\alpha) = 16\alpha^{1.5}(1 + 56\alpha^3)$, when $0.06 < \alpha < 0.3$.

Kuwabara and Happel obtained the solution to Stokes equations with viscous fluid flowing through the randomly distributed cylinder array, respectively. The expression given by Kuwabara was (Kuwabara, 1959):

$$\frac{\Delta pA(R_f)^2}{\mu QL} = \frac{8\alpha}{-\ln\alpha + 2\alpha - \alpha^2/2 - 3/2} \tag{27}$$

Happel obtained his expression as follows (Happel, 1959):

$$\frac{\Delta pA(R_f)^2}{\mu QL} = \frac{8\alpha}{-\ln\alpha - (1-\alpha^2)/(1+\alpha^2)} \tag{28}$$

Expression of Resistance in Simulation

To investigate the performance of two filter media models, horizontal sampling line was set with two terminal sampling points placed at the midpoint of AH and DE, respectively. The simulation resistance value Δp can be expressed as follows:

$$\Delta p = p_{in} - p_{out} \tag{29}$$

where Δp is the pressure drop across a filter media with a thickness L. p_{in} and p_{out} are the static pressures at inlet and outlet of media, respectively.

To compare with the experimental and analytical data, the dimensionless resistance value Δp_1 is required to be converted to the actual resistance Δp_p. Eq. (30) can be used, where subscript p denotes the dimensionless parameters and subscript 1 denotes the actual parameters.

$$\frac{\Delta p_p}{\rho_p U_p^2/2} = \frac{\Delta p_1}{\rho_1 U_1^2/2} \tag{30}$$

Test Rig for Experiment

Experiments were performed on filter media test rig in the Aerosol Technology and Filter Testing Laboratory, Politecnico di Torino, Italy (Zhou *et al*., 2010).

Indoor air from the laboratory was delivered through the supply fan and exhaust fan. The flow rate of the test rig can be varied between 6 $m^3 s^{-1}$ and 60 $m^3 s^{-1}$ by the inverters. The incoming air passed through the absolute air filter (HEPA). The clean air was mixed with the aerosol in the mixing box (aerosol-air mixing chamber). Aerosol was generated with a Laskin nozzle which was put inside a container. Then aerosol was injected towards the mixing box through a plastic pipeline with diameter 65 mm. The mixing box was a cubic with the side length 495 mm.

The holder chamber for the filter media was also s cubic. Its side length was 300 mm. The section for measurement of the flow rate with the manometer was placed at the downstream of this holder chamber.

Two aerosol sampling pipelines were set upstream and downstream of the holder chamber for the media. The diameters of these two sampling probes were chosen according to the isokinetic sampling theory.

The pressure drop was measured with a differential manometer. Lax-X optical particle counter manufactured by Particle Measuring Systems Co. Ltd was used to measure the upstream and downstream particle concentrations, which were applied to obtain the efficiency value of the media. The schematic diagram of the test rig is shown in Fig. 4.

RESULTS AND DISCUSSION

Validation of the Mesh Dependence

Before extracting the information about the flow field of filter media, the validation of the mesh dependence was studied to ensure the accuracy of the simulations. For the convenience of comparison, we take the mesh density on the single fiber with diameter D = 2 μm as an example. Table 3 lists four kinds of mesh densities on single fiber.

The comparison of the resistance values with various mesh densities are shown in Fig. 5.

Table 3. Different mesh densities on single fiber with diameter D = 2 μm.

Different mesh densities	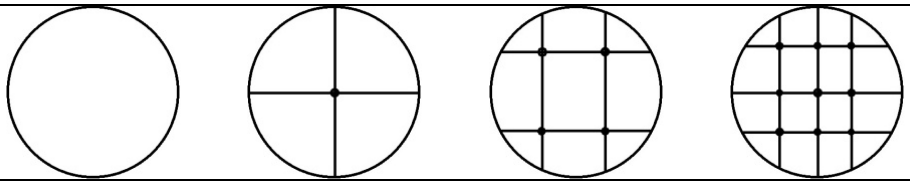			
Mesh density on single fiber	1	4	9	16

Table 4. Cases with different boundary conditions.

Case	Upper and lower boundaries	Fiber surface	Inlet	Outlet
A	Non-equilibrium extrapolation	No-slip	Velocity inlet	Fully developed
B	Non-equilibrium extrapolation	slip	Velocity inlet	Fully developed
C	Periodic	No-slip	Velocity inlet	Fully developed
D	Periodic	slip	Velocity inlet	Fully developed

It is shown in Fig. 5 that the resistance of media F6 differs a lot when the number of mesh occupied by a single fiber with diameter 2 μm varies from 1 to 4. When the mesh density is bigger than 4, the resistance is very close to each other, i.e., the resistance can reach stable when the meshing of media F6 is 670 × 75. Therefore, in order to ensure the accuracy of the simulation, the final selected mesh densities for media F6 was 670 × 75.

Velocity Magnitude Contour

From the velocity magnitude contours shown in Fig. 6, obvious flow channels with higher velocity appear in the middle of the media models. In the randomly arranged fibers, the velocity will increase a lot when the space between fibers turns larger, i.e., the warm color areas. Likewise, the velocity is relatively small when fibers are densely occupied, i.e., the cool color areas. For the case where inter-space between fibers is large, air flow channels will be formed through these spaces and the average velocity through the channel is comparatively large. This was also discovered by Chen and Papathanasiou (2008).

Validation of Resistance

Comparison of Resistance with Non-Equilibrium Extrapolation Schemes

Simulation was performed to obtain the resistance of filter media F6 with various inlet velocities. The resistance Δp from numerical simulation was validated against experimental and analytical data. Analytical results from Davies (1973), Kuwabara (1959) and Happel (1959) were included. Table 4 illustrates cases with different boundary conditions during simulation.

In Fig. 7, both case A and case B corresponded to situations where the upper and lower boundaries adopted non-equilibrium extrapolation format. Case A took no-slip boundary condition on fiber surface and case B took slip boundary condition. For case A, it is shown that the resistance values of two filter media almost increased linearly with the inlet velocity, which agrees with the Darcy's law. For case B, the variation of resistance values with the inlet velocity also showed the same growth trend.

The resistance values from expressions by Happel and Davies were both lower than the experimental values, whereas the values from Kuwabara's expressions were closest to it. The resistance values Δp for case B were much lower than that for case A. In other words, aerodynamic slip makes a significant decrease in the resistance for filter media.

Thus, it is essential to pay attention to the slippage effect during the study on the flow field of fibrous media.

The above simulation results were obtained when the upper and lower boundaries adopt non-equilibrium extrapolation format. It can be seen that the resistance values Δp for case B still have a large difference from the experimental results. Therefore, the influence of the boundary conditions on the F6 model was further investigated.

Comparison of Resistance with Periodic Schemes

Since the upper and lower boundaries can be regarded as infinitely far as to have negligible influence on the flow field, periodic boundary format was also investigated. This treatment is in line with the actual situation, which is shown in Fig. 8. It cannot only reduce the impact of the upper and lower wall on the flow field, but also ensure the conservation of mass and energy for entire system (He *et al*., 2009).

In Fig. 9, case C took no-slip boundary condition on fiber surface and case D took slip boundary condition. The resistance values Δp for case D were smaller than that for case C. Compared with the results in Fig. 7, the resistance values of simulation were much smaller, which show less influence by upper and lower boundaries. The resistance values for case C were higher than the experimental data. However, for case D, the resistance values of media F6 were closer to the experimental data with the increase of the inlet velocity. Under various inlet velocities, the simulation results are all between the two dash lines, i.e., within the range of the deviation degree. The resistance values obtained have a good agreement with the experimental data.

It is shown that only the treatment of the upper and lower boundaries can exert a large influence on the simulation results. For laminar flow with low Reynolds number, the initial conditions of the flow field have little effect on the final results, while the boundary conditions may have more impact on it, together with numerical stability and computational efficiency.

The dimensionless resistance reduction Π is defined as (Yu *et al*., 2015):

$$\Pi = \frac{\Delta p_{no-slip} - \Delta p_{slip}}{\Delta p_{no-slip}} \times 100\% \tag{31}$$

The numerical relationship between Π and the inlet velocity reflects the degree of resistance decrease, as shown in Fig. 10.

Compared with the simulation results for case C and case D, the dimensionless resistance reduction Π of media F6 was obtained. Generally, with the increase of the inlet velocity U, Π of media F6 decreased first and then increased. Within the inlet velocity range, the maximal reduction Π of media F6 was 33.7% when U was the smallest. Moreover, Π of media F6 decreased to the minimum value 25.0% when $U = 0.046$ m s^{-1}. In short, within a certain range of flow rate, the application of slip boundary can bring a

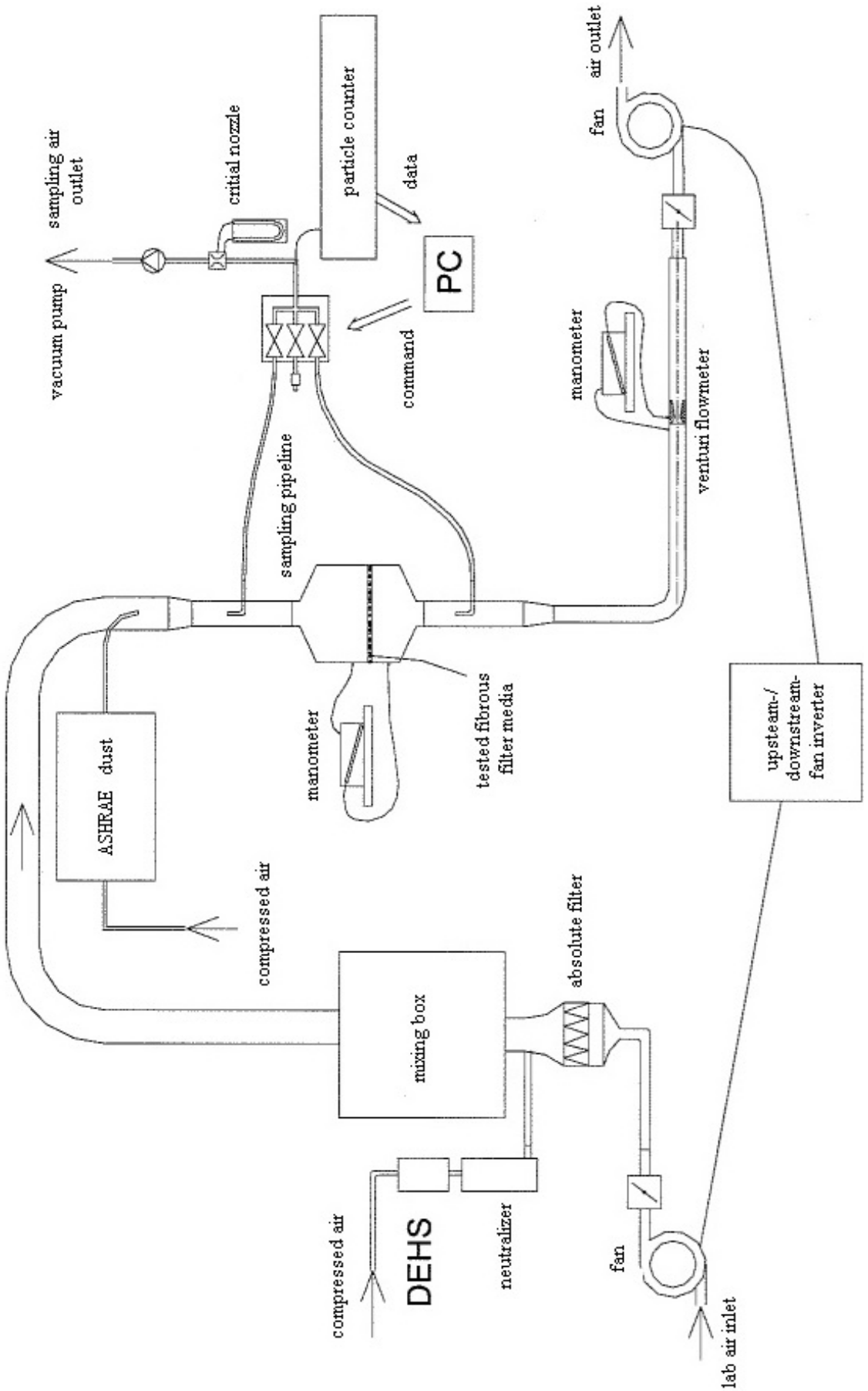

Fig. 4. Schematic diagram of the test rig.

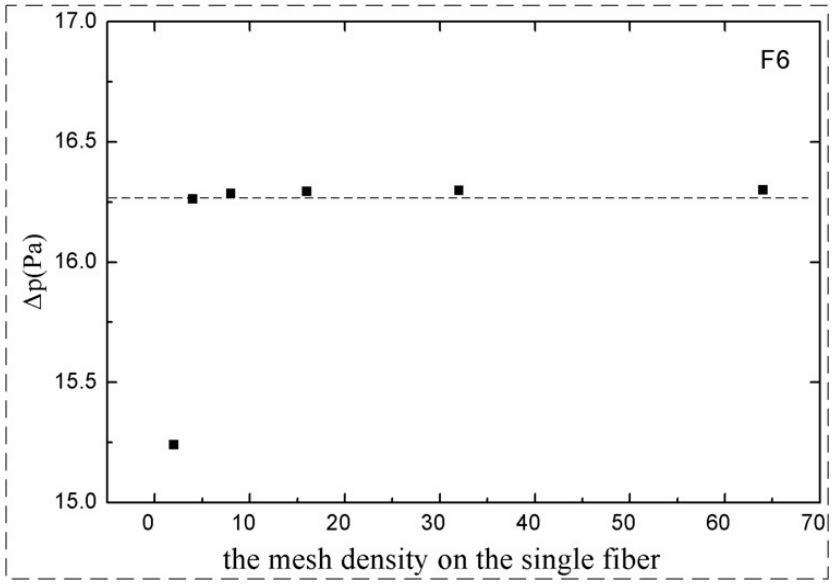

Fig. 5. Grid independence test for resistance.

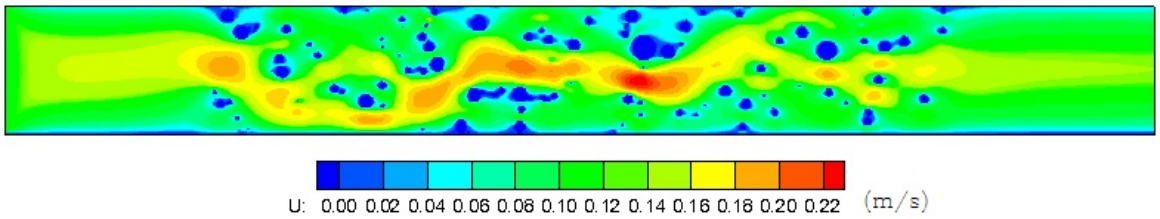

Fig. 6. Velocity magnitude contours with slip boundary conditions.

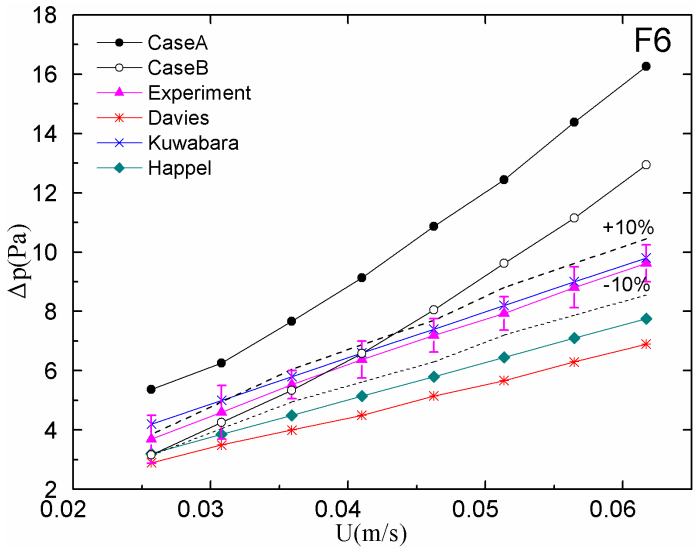

Fig. 7. The resistance Δp versus inlet velocity U (Cases A & B).

decline rate of resistance for media F6 to be 25.0%.

From Fig. 10 it is shown that slippage effect turns significant when the inlet velocity is low enough. For the case of smallest inlet velocity, the boundary layer around fibers is comparatively thicker than that of large inlet velocity. Therefore, the implementation of slip boundary condition on fiber surface will have more significant effect on the flow field inside fibrous media, which results in the larger relative difference of resistance values between slip and no-slip boundary conditions. As the inlet velocity increase, the thickness of the boundary layer near the wall will be reduced. This means that when the no-slip wall boundary is implemented on the fiber surface, the influence of the boundary layer on the pressure drop of the model will be

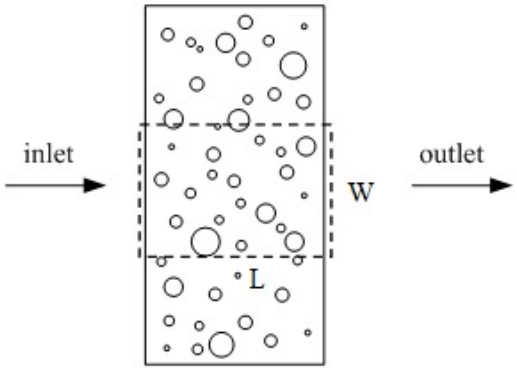

Fig. 8. The cross section of filter media and the investigated region.

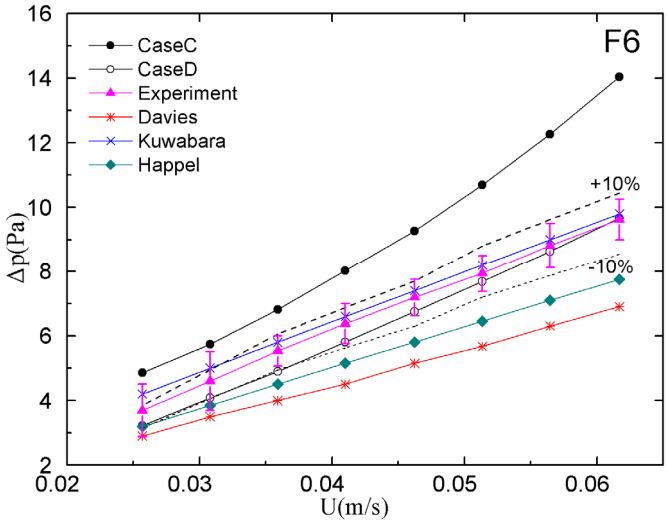

Fig. 9. The resistance Δp versus inlet velocity U (Cases C & D).

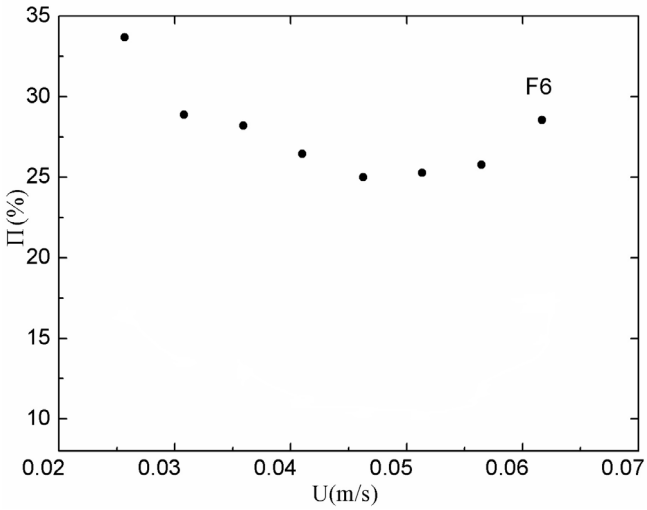

Fig. 10. The dimensionless resistance reduction Π versus the inlet velocity U.

decreased with the reduced thinner boundary layer. Therefore, the difference between no-slip and slip boundary conditions region forms at the downstream of the cylinder and the fluctuation of the wake flow becomes fierce. The possibility of vortex shedding becomes larger. As the turbulence in this case becomes smaller.

However, as the inlet velocity further increases, the wake intensity increases, the drag force on the fiber when no-slip boundary is applied will be increased. On the contrary, the phenomenon for the fluctuation of the wake flow will be

reduced if the slip boundary is utilized. This will reduce the pressure drop of the model. In this case, the difference between no-slip and slip boundary conditions in this case becomes larger again.

Validation of Efficiency

Experimental Value of Efficiency

Table 5 illustrates the fractional efficiency of media F6 with the filtration velocity 0.0617 m s^{-1}.

Simulated Value of Efficiency

After the stabilized flow field was obtained, 500 particles with diameter 0.1 μm, 1 μm and 5 μm were injected at the entrance of the filter media, respectively. In order to reduce the influence of the initial particle positions, independent random numbers were generated so that particles were distributed randomly in the region $1 \le x \le 120$ μm and $1 \le y \le 75$ μm. The density of the simulated particles was 912 kg m^{-3}, which corresponds with that of DEHS aerosol. The processes for particle movement and capture were monitored. Once particles contact the fiber surface, they were considered to be captured and then assumed to disappear.

Figs. 11–13 present the state diagram of particles released at the entrance, particles near the fibers and the whole condition inside the media, respectively.

According to Table 5, the experimental efficiency for particles with diameter between 0.75 μm and 1.00 μm reached 23.4% ± 2.8%, while that for particles with diameter between 1.50 μm and 2.00 μm reached 38.1% ± 4.1%. Fig. 14 illustrates the comparison of efficiency between simulation and experiment. The mean diameter in each size range interval shown in Table 5 is used for plotting Fig. 14. It is equal to the geometric average of the lower and upper border diameter. It should be noted that in the experiment data, the filtration efficiency for particles with diameter 0.1 μm was less than that for 0.2 μm. When the measurement error

Table 5. Filtration efficiency of media F6 with the rated filtration velocity 0.0617 m s^{-1}.

Lower diameter (μm)	Upper diameter (μm)	Efficiency (%)	Standard deviation (%)
0.10	0.12	8.8	4.2
0.15	0.20	10.7	1.1
0.45	0.60	16.1	2.5
0.75	1.00	23.4	2.8
1.50	2.00	38.1	4.1
2.00	3.00	53.5	2.4
4.50	6.00	65.7	24.9

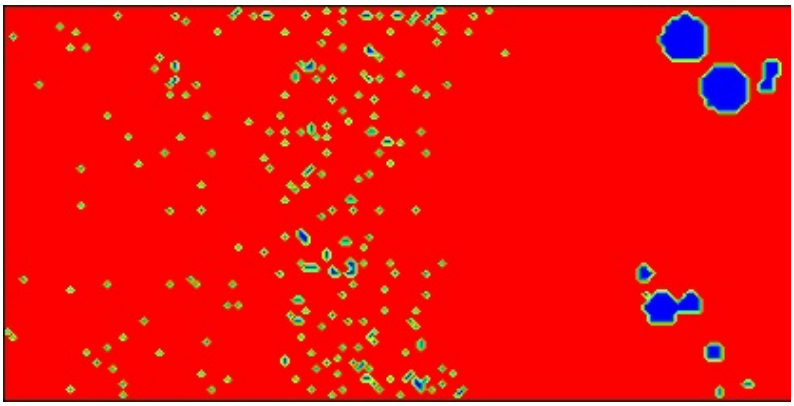

Fig. 11. Schematic diagram of particles released at the entrance of media.

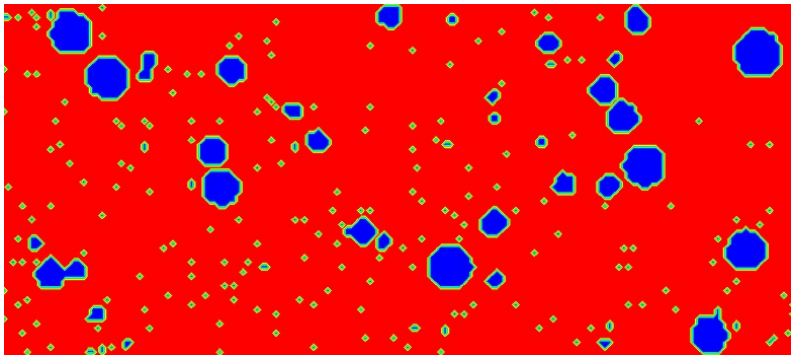

Fig. 12. Schematic diagram for the partially enlarged view of particles in the media.

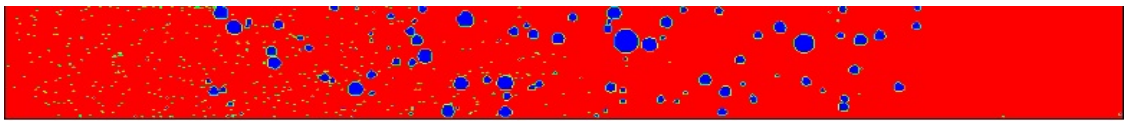

Fig. 13. Schematic diagram of particles in the media.

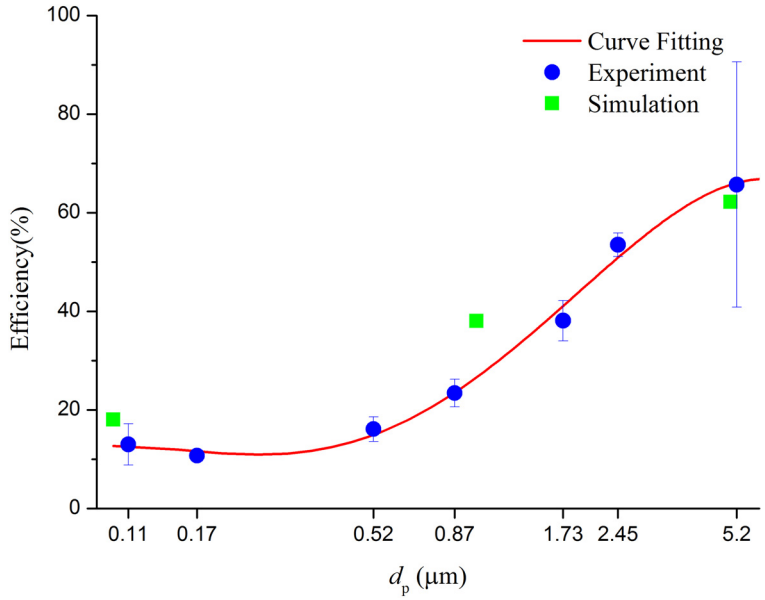

Fig. 14. Comparison of efficiency between experiment and simulation.

is considered, the summation of the average efficiency and deviation is used to plot the data corresponding 0.1 μm in Fig. 14. The simulated filtration efficiency for particles with diameter 1 μm was 38.0% under the filtration velocity 0.0617 m s^{-1}. The difference between simulation and experiment for this particle diameter is nor large. However, it is found that the simulated particle capture efficiency for particles with diameter 5 μm is smaller than the experimental data. The possible reason is that in real fibrous filter media, binder is usually used for fixing the place of fibers. The existence of binder may increase the actual particle capture efficiency. This is why the experimental data is larger than the simulated value with the current model. Therefore, the binder is suggested to be added in the future model of the media.

CONCLUSIONS

By applying LB method for the truncated log-normal distribution model of fibrous media F6, the influence of boundary conditions on the resistance of the media was investigated. Compared with the no-slip boundary condition, the simulated resistance with the implementation of slip boundary condition on fiber surface agrees well with the experimental data. For low *Re* number flow inside the fibrous filter media, the resistance of the upper and lower boundaries with the periodic scheme is much closer to the experimental value. This reflects the real condition of the fibrous media. In short, the influence of boundary condition is larger than that of the initial condition on the simulated results.

Moreover, Kuwabara's expression is the best to describe the resistance of the fibrous filter media, compared with these expressions by Happel and Davies.

It should be noted that the *Re* number in the simulation on the simplified 2D fiber model is the same as that in the experiment. This dimensionless parameter is one important factor for the similarity between simulation and experiment.

By validating the resistance and the filtration efficiency on the truncated log-normal model, it is found that the LB method can be used to predict the performance of the fibrous filter media. Meanwhile, the model to include the effect of binder in fibrous media is needed in future study.

ACKNOWLEDGMENTS

Thanks are given to Assoc. Prof. Paolo Tronville from Politecnico di Torino and Mr. Richard Rivers (ASHRAE Fellow) from EQS Inc., Louisville, USA for assistance with the experiments and valuable discussion. We also thank Zhibo Dong for the detailed and valuable discussion of the code. Acknowledgement is also sent to reviewers for their constructive suggestions.

This work is financially supported by the National Natural Science Foundation of China (No.51508267), the Natural Science Foundation of Jiangsu Province (No.BK20130946), Innovative research projects for college graduate student from Jiangsu Province in 2016 (SJLX16_0309) and the Scientific Research Foundation from Nanjing Tech University (No. 44214122).

REFERENCES

Agarwal, R.K., Chusak, L. and Morgan, B. (2009). Lattice boltzmann simulations of slip flow of newtonian and non-newtonian fluids in microgeometries. Proceedings of the 47th AIAA Aerospace Sciences Meeting Including the New Horizons Forum and Aerospace Exposition, Florida, U.S.A.

Ansumali, S. and Karlin, I.V. (2002). Kinetic boundary conditions in the lattice boltzmann method. *Phys. Rev. E* 66: 064502.

Bang, J.G. and Yoon, W.S. (2014). Stochastic analysis of a collection process of submicron particles on a single fiber accounting for the changes in flow field due to particle collection. *J. Mech. Sci. Technol.* 28: 3719–3732.

Chai, Z.H., Lu, J.H., Shi, B.C. and Guo, Z.L. (2011). Gas slippage effect on the permeability of circular cylinders in a square array. *Int. J. Heat Mass Transfer* 54: 3009–3014.

Chen, X.M. and Papathanasiou, T.D. (2008). The transverse permeability of disordered fiber arrays: A statistical correlation in terms of the mean nearest interfiber spacing. *Transp. Porous Media* 71: 233–251.

Chen, Y.L., Cao, X.D. and Zhu, K.Q. (2009). A gray lattice Boltzmann model for power-law fluid and its application in the study of slip velocity at porous interface. *J. Non-Newtonian Fluid Mech.* 159: 130–136.

Cho, H.J., Jeong, N.Y. and Sung, H.J. (2013). Permeability of microscale fibrous porous media using the lattice Boltzmann method. *Int. J. Heat Fluid Flow* 44: 435–443.

Davies, C.N. (1973). *Air Filtration*, Academic Press, New York.

Fotovati, S., Tafreshi, H.V. and Pourdeyhimi, B. (2012). A macroscale model for simulating pressure drop and collection efficiency of pleated filters over time. *Sep. Purif. Technol.* 98: 344–355.

Guo, Z.L., Zheng, C.G. and Shi, B.C. (2002). Discrete lattice effects on the forcing term in the lattice boltzmann method. *Phys. Rev. E* 65: 046308.

Hadjiconstantinou, N.G. (2003). Comment on Cercignani's secondorder slip coefficient. *Phys. Fluids* 15: 2352–2354.

Happel, J. (1959). Viscous flow in arrays of cylinders. *AIChE J.* 5: 474–477.

He, Y.L., Wang, Y. and Li, Q. (2009). *Lattice Boltzmann Method: Theory and Applications*, Science Press, Beijing (in Chinese).

Hosseini, S.A. and Tafreshi, H.V. (2010). Modeling permeability of 3-D nanofiber media in slip flow regime. *Chem. Eng. Sci.* 65: 2249–2254.

Hosseini, S.A. and Tafreshi, H.V. (2011). On the importance of fibers' cross-sectional shape for air filters operating in the slip flow regime. *Powder Technol.* 212: 425–431.

Huang, H., Wang, K. and Zhao, H. (2016). Numerical study of pressure drop and diffusional collection efficiency of several typical noncircular fibers in filtration. *Powder Technol.* 292: 232–241.

Joubert, A., Laborde, J.C., Bouilloux, L., Chazelet, S. and Thomas, D. (2011). Modelling the pressure drop across HEPA filters during cake filtration in the presence of humidity. *Chem. Eng.* 166: 616–623.

Karniadakis, G.E.M., Beskok, A. and Gad-El-Hak, M. (2002). *Micro Flows: Fundamentals and simulation*, Springer Press, New York.

Kim, J.Y., Gao, S., Yermakov, M., Elmashae, Y., He, X.J., Reponen, T. and Grinshpun, S.A. (2016). Performance of electret filters for use in a heating, ventilation and air conditioning system and an automotive cabin against combustion and NaCl Particles. *Aerosol Air Qual. Res.* 16: 1523–1531.

Kim, S.H., Pitsch, H. and Boyd, I.D. (2008). Slip velocity and Knudsen layer in the lattice Boltzmann method for microscale flows. *Phys. Rev. E* 77: 026704.

Kirsh, V.A. and Shabatin, A.V. (2015). Deposition of nanoparticles in model multilayer fibrous filters with three-dimensional structure. *Colloid J.* 77: 32–37.

Kuwabara, S. (1959). The forces experienced by randomly distributed parallel circular cylinders or spheres in a viscous flow at small Reynolds numbers. *J. Phys. Soc. Jpn.* 14: 527–532.

Li, B.W., Yao, Z.H. and Hao, P.F. (2015). Incompressible LBGK simulation of flow characteristics in a microchannel with patterned superhydrophobic surfaces. *Appl. Math. Modell* 39: 300–308.

Li, Q., He, Y.L., Tang, G.H. and Tao, W.Q. (2011). Lattice Boltzmann modeling of microchannel flows in the transition flow regime. *Microfluid. Nanofluid.* 10: 607–618.

Neumann, P. and Rohrmann, T. (2012). Lattice Boltzmann simulations in the slip and transition flow regime with the Peano framework. *J. Fluid Dynam.* 2: 101–110.

Niu, X.D., Shu, C. and Chew, Y.T. (2004). A lattice Boltzmann BGK model for simulation of microflows. *Europhys. Lett.* 67: 600–606.

Przekop, R. and Gradoń, L. (2008). Deposition and filtration of nanoparticles in the composites of nano- and microsized fibers. *Aerosol Sci. Technol.* 42: 483–493.

Przekop, R. and Gradoń, L. (2011). Non-steady-state aerosol filtration in nanostructured fibrous media. *Philos. Trans. R. Soc. London, Ser. A* 369: 2476–2484.

Qian, F.P., Huang, N.J., Zhu, X.J. and Lu, J.L. (2013). Numerical study of the gas–solid flow characteristic of fibrous media based on SEM using CFD–DEM. *Powder Technol.* 249: 63–70.

Rebaï, M., Drolet, F., Vidal, D., Vadeiko I. and Bertrand, F. (2011). A Lattice Boltzmann approach for predicting the capture efficiency of random fibrous media. *Asia-Pac. J. Chem. Eng.* 6: 29–37.

Sbragaglia, M. and Succi, S. (2005). Analytical calculation of slip flow in lattice Boltzmann models with kinetic boundary conditions. *Phys. Fluids* 17: 093602.

Succi, S. (2002). Mesoscopic modeling of slip motion at fluid-solid interfaces with heterogeneous catalysis. *Phys. Rev. Lett.* 89: 064502.

Tang, G.H., Tao, W.Q. and He, Y.L. (2004). Lattice Boltzmann method for simulating gas flow in microchannels. *Int. J. Mod. Phys. C* 15: 335–347.

Tang, G.H., Tao, W.Q. and He, Y.L. (2005). Lattice

Boltzmann method for gaseous microflows using kinetic theory boundary conditions. *Phys. Fluids* 17: 058101.

Tian, Z.W., Zheng, C.G. and Wang, X.M. (2009). Lattice Boltzmann Simulation of gas micro-flows in transitional regime. *Chin. J. Theor. Appl. Mech.* 41: 828–834.

Tronville, P. and Rivers, R. (2005). Numerical modeling of the flow resistance of fibrous air filter media having random fiber diameter. Proc. Filtech 2005 Conference, Wiesbaden, Germany, Vol. 2, pp. 261–268.

Wang, H., Zhao, H., Guo, Z. and Zheng, C. (2012). Numerical simulation of particle capture process of fibrous filters using Lattice Boltzmann two-phase flow model. *Powder Technol.* 227: 111–122.

Wang, H., Zhao, H., Wang, K., He, Y. and Zheng C. (2013). Simulation of filtration process for multi-fiber filter using the Lattice-Boltzmann two-phase flow model. *J. Aerosol Sci.* 66: 164–178.

Wang, H.L., Chai, Z.H. and Guo, Z.L. (2009). Lattice Boltzmann simulation on gas seepage in dense porous media. *J. Comput. Phys.* 26: 389–395 (in Chinese).

Xu, B., Wu, Y. and Cui, P.Y. (2014). Semi-analytical and computational investigation of different dust loading strucxtures affecting the performance of a fibrous air filter. *Particuology* 13: 60–65.

Yamamoto, K. and Yamauchi, K. (2013). Numerical simulation of continuously regenerating diesel particulate filter. *Proc. Combust. Inst*. 34: 3083–3090.

Yamamoto, K., Satake, S. and Yamashita, H. (2009). Microstructure and particle-laden flow in diesel particulate filter. *Int. J. Therm. Sci.* 48: 303–307.

Yu, Z.J., Liu, X.H. and Kuang, G.Z. (2015). Water slip flow in superhydrophobic microtubes within laminar flow region. *Chin. J. Chem. Eng.* 23: 763–768.

Zhao, S. and Povitsky, A. (2009). Method of fundamental solutions for partial-slip fibrous filtration flows. *Int. J. Numer. Methods Fluids* 61: 255–274.

Zheng, L., Guo, Z.L. and Shi, B.C. (2012). Microscale boundary conditions of the lattice Boltzmann equation method for simulating microtube flows. *Phys. Rev. E* 86: 016712.

Zhou, B., Tronville, P. and Rivers, R. (2009). Generation of 2-dimensional models for CFD simulation of fibrous filter media with binder. *Fibers Polym.* 10: 526–538.

Zhou, B., Tronville, P., Rivers, R. and Zhang, X.S. (2010). Numerical study of pressure drop for a new fibrous media model. *J. Southeast Univ. (English Edition)* 26: 311–315.

Zhou, B., Tronville, P. and Rivers, R. (2013). Realistic air filter media performance simulation. Part II: Beyond finite-volume computational fluid dynamics procedures. *HVAC&R Res.* 19: 503–512.

Received for review, December 22, 2016
Revised, February 22, 2017
Accepted, February 25, 2017